Supporting information

Biogenic derived nanoparticles modulate mitochondrial function in cardiomyocytes

Xiaolan Zheng§, Tianyou Wang§, Jixing Gong§, Peng Yang, Yulin Zhang, Yue Zhang, Nan Cao, Kaiyu Zhou, Yiwen Li, Yimin Hua, Donghui Zhang*, Zhipeng Gu*, Yifei Li*

Xiaolan Zheng, Yulin Zhang, Yue Zhang, Kaiyu Zhou, Yimin Hua, Yifei Li

Key Laboratory of Birth Defects and Related Diseases of Women and Children of MOE, Department of Pediatrics, West China Second University Hospital

Sichuan University

Chengdu, Sichuan 610041, China

Email: liyfwcsh@scu.edu.cn (Yifei Li)

Tianyou Wang, Peng Yang, Yiwen Li, Zhipeng Gu

College of Polymer Science and Engineering, State Key Laboratory of Polymer Materials Engineering

Sichuan University

Chengdu, 610065, China

Email: guzhipeng2019@scu.edu.cn (Zhipeng Gu)

Jixing Gong, Donghui Zhang

State Key Laboratory of Biocatalysis and Enzyme Engineering, School of Life Science

Hubei University

Wuhan, 430062, China

Email: dongh.zhang@hubu.edu.cn (Donghui Zhang)

Jixing Gong, Nan Cao

Advanced Medical Technology Center, Zhongshan School of Medicine and the First Affiliated Hospital,

Sun Yat-Sen University,

Guangdong 510080, China

§ These authors contributed equally

Running title: NPs protects CMs by modulating mitochondria

Stability of PPP NPs

To demonstrate the stability of PPP NPs for further biomedical application, the various mediums such as deionized water, phosphate buffered saline (PBS, pH=7.4) and culture medium (10 % fetal bovine serum in dulbecco's modified eagle medium) were utilized and the dynamic light scattering (DLS) sizes were assayed and recorded with different time up to 48 h. The PPP-2 NPs were set as example and the concentration was 0.5 mg/mL.

Free radical scavenging abilities of PPP NPs

To confirm the strong free radical scavenging abilities of PPP NPs, the DPPH, ABTS, H_2O_2 as well as hydroxyl radical assay were conducted with various concentrations of PPP NPs and incubation time.

DPPH assay: Briefly, DPPH solution was first prepared with the concentration of 1.0 mM in ethanol, and PPP-i (i=1-4) NPs with the various concentrations were also prepared for further assays. The 300 μL DPPH solution and 100 μL samples were added

into 2600 μL ethanol, and corresponding absorbance at 517 nm was recorded with different time up to 30 min. Subsequently, the DPPH free radical scavenging abilities with different NPs concentrations were assayed and the scavenging ratios were calculated after 30 min co-incubation.

ABTS assay: Briefly, ABTS solution was prepared with 54.04 mg ABTS and 9.93 mg potassium peroxodisulfate dissolved in 15 mL deionized water, then the above solution was mildly stirred in dark at room temperature overnight. PPP-i (i=1-4) NPs with various concentrations were also prepared for further assays. The 100 μL ABTS solution and 100 μL samples were added into 2800 μL deionized water, and corresponding absorbance at 734 nm was recorded with different time up to 30 min. Subsequently, the ABTS free radical scavenging abilities with different NPs concentrations were assayed and the scavenging ratios were calculated after 30 min co-incubation.

H_2O_2 assay: Briefly, H_2O_2 solution with the concentration of 50 mM and PPP-i (i=1~4) NPs with various concentrations were freshly prepared. The 200 μL H_2O_2 solution and 100 μL samples were added into 2600 μL deionized water, and corresponding absorbance at 240 nm was recorded with different time up to 30 min. Subsequently, the H_2O_2 scavenging abilities with different NPs concentrations were assayed and the scavenging ratios were calculated after 30 min co-incubation.

Hydroxyl radical assay: Briefly, hydroxyl radical was produced with the reaction between $FeSO_4$ and H_2O_2, and 1 mM $FeSO_4$, 2.5 mM H_2O_2, 0.75 mM salicylic acid and PPP NPs with different concentrations were prepared in PBS. The corresponding

absorbance at 510 nm was recorded with different time up to 30 min. Subsequently, the hydroxyl radical scavenging abilities with different NPs concentrations were assayed and the scavenging ratios were calculated after 30 min co-incubation.

Characterization

Scanning Electron Microscope (SEM) images were obtained with a Nova Nano SEM 450 microscope. Hydrodynamic Diameter (DH) testing was carried out by dynamic light scattering (DLS) and Zeta Potentials (ZP) was tested by Malvern Nano ZS ZEN3690 instrument. The samples were prepared with a substrate of mice and fully dried before testing. Electron energy-loss spectroscopy (EELS) mapping testing was carried out with FEI Tecnai F20 and 200 kV accelerating voltage was applied. Fourier-transform infrared spectroscopy (FTIR) was carried out with the Perkin-Elmer spectrum one B system by KBr pellets method and the resolution was 4.0 cm-1. UV-Vis spectroscopy experiment was performed by PerkinElmer Lambda 650 UV/Vis spectrophotometer with slit of 2 nm. Electrospray ionization mass spectrometry (ESI-MS) spectrum was carried out by the Applied Biosystems Biosystems API 2000 with cationic mode electrospray ionization at a flow rate of 10 μL/min, spray voltage of 5 kV as well as auxiliary and sheath pressure of 45 psi. X-ray photoelectron spectroscopy (XPS) was carried out by PHI Quantera SXM spectrometer using Al Ka radiation and spectra were obtained at the pass energy of 160 eV for survey spectra and 20 eV high-resolution spectra of C 1s, O 1s regions with the 300 ms dwell time. Electron Paramagnetic Resonance (EPR) was carried out by the Bruker EPR EMX Plus. The spectrometer was performed at X-Band (9.85GHz) and the spectrum was harvested

with 100 kHz field modulation at the power of 0.1 mW.

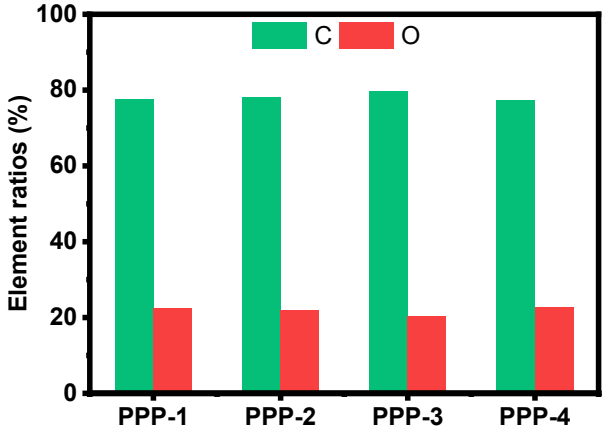

Figure S1. The element ratios of C and O elements in the PPP-1~4 NPs.

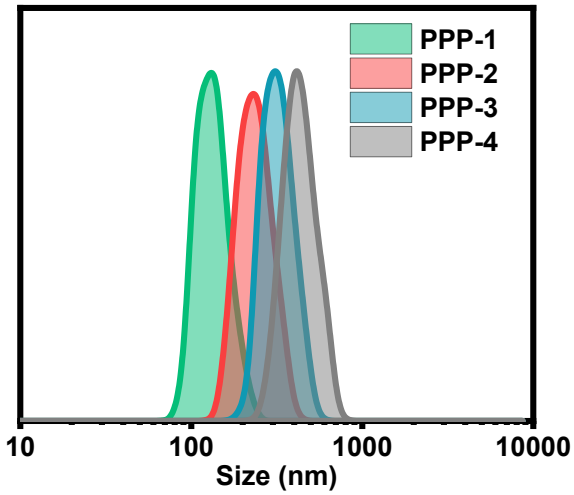

Figure S2. The DLS traces of PPP-i (i=1-4) NPs

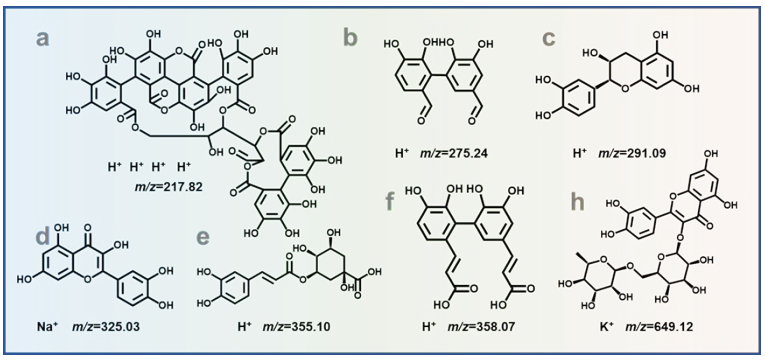

Figure S3. The proposed structures of pomegranate peel polyphenol speculated from ESI-MS spectra.

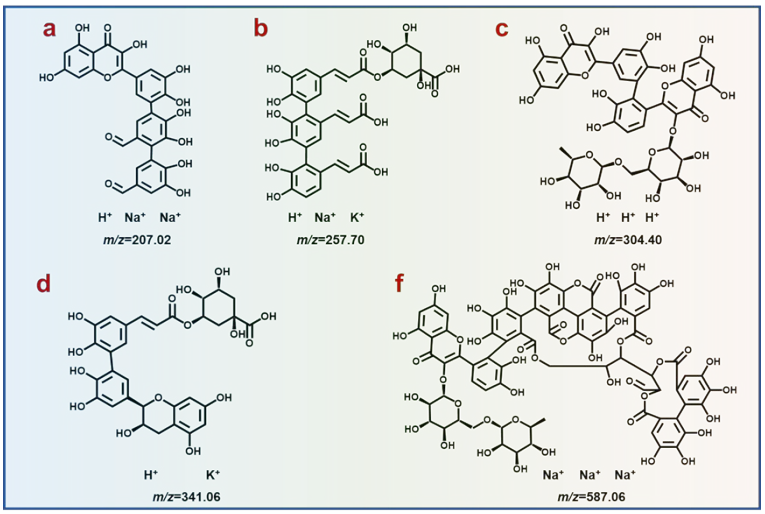

Figure S4. The proposed structures of PPP-2 NPs intermediate products speculated from ESI-MS spectra.

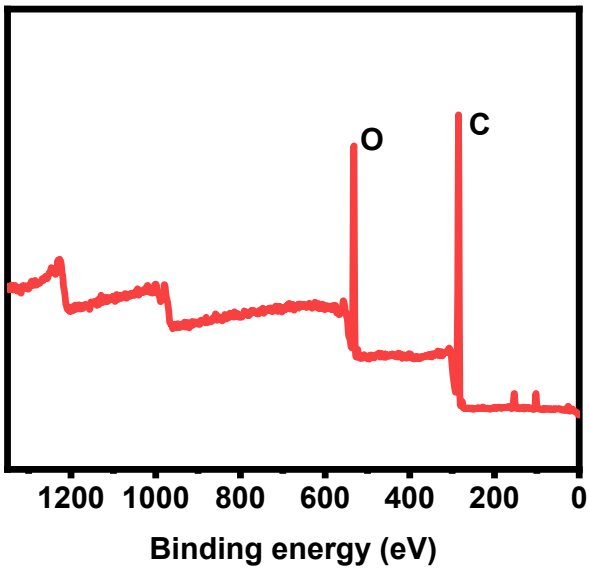

Figure S5. XPS result of PPP-2 NPs.

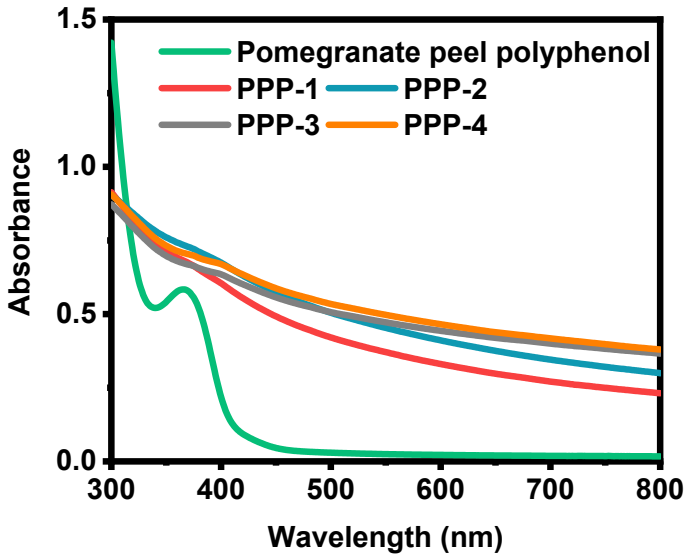

Figure S6. UV-vis spectra of pomegranate peel polyphenol as well as PPP-i (i=1-4) NPs.

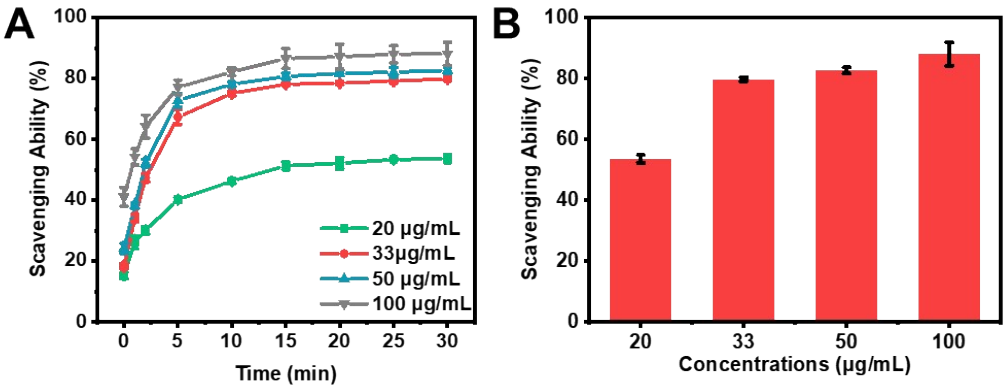

Figure S7. (A) ROS scavenging curves toward DPPH with time up to 30 mins of PPP-2 NPs with different concentrations. (B) ROS scavenging abilities toward DPPH after 30 mins of PPP-2 NPs with different concentrations.

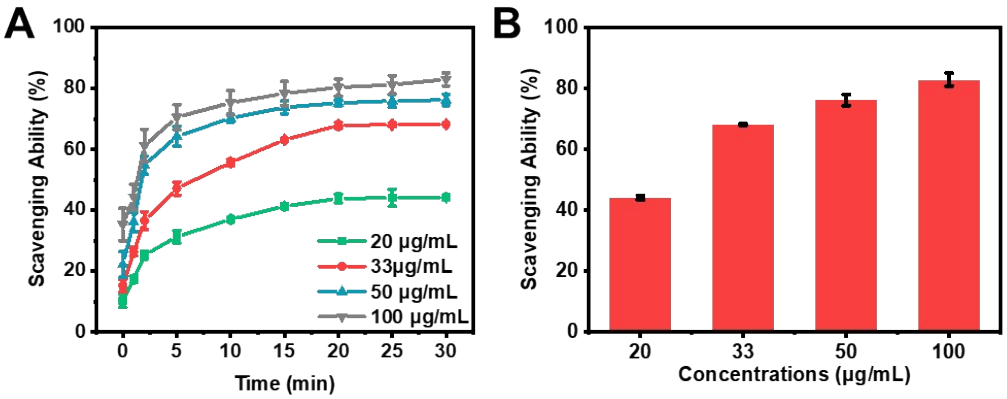

Figure S8. (A) ROS scavenging curves toward ABTS with time up to 30 mins of PPP-2 NPs with different concentrations. (B) ROS scavenging abilities toward ABTS after 30 mins of PPP-2 NPs with different concentrations.

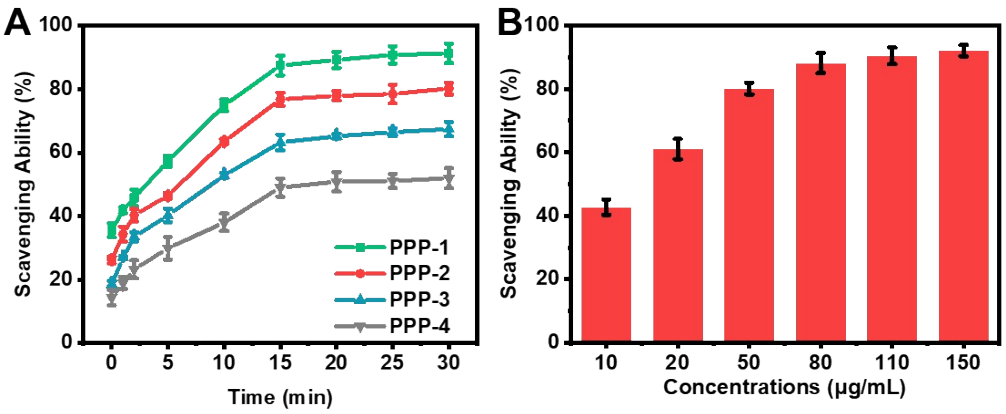

Figure S9. (A) ROS scavenging curves toward hydrogen peroxide with time up to 30 mins of PPP-i (i=1-4) NPs. (B) ROS scavenging abilities toward hydrogen peroxide after 30 mins of PPP-2 NPs with different concentrations.

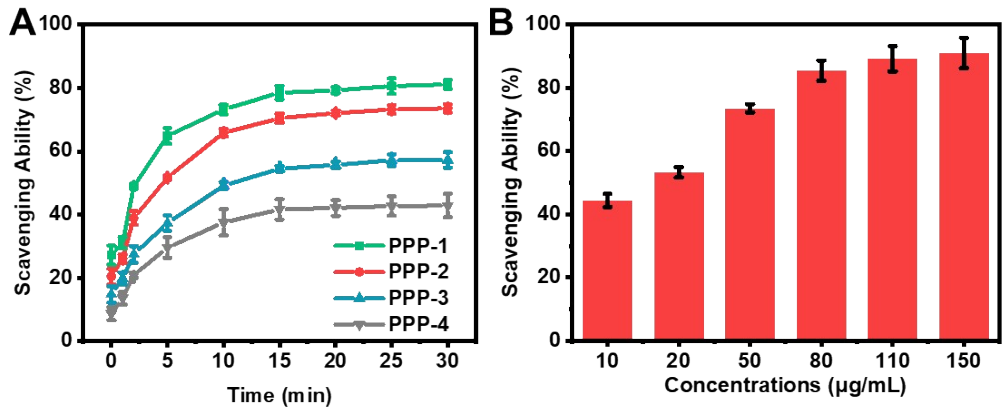

Figure S10. (A) ROS scavenging curves toward hydroxyl radical with time up to 30 mins of PPP-i (i=1-4) NPs. (B) ROS scavenging abilities toward hydroxyl radical after 30 mins of PPP-2 NPs with different concentrations.

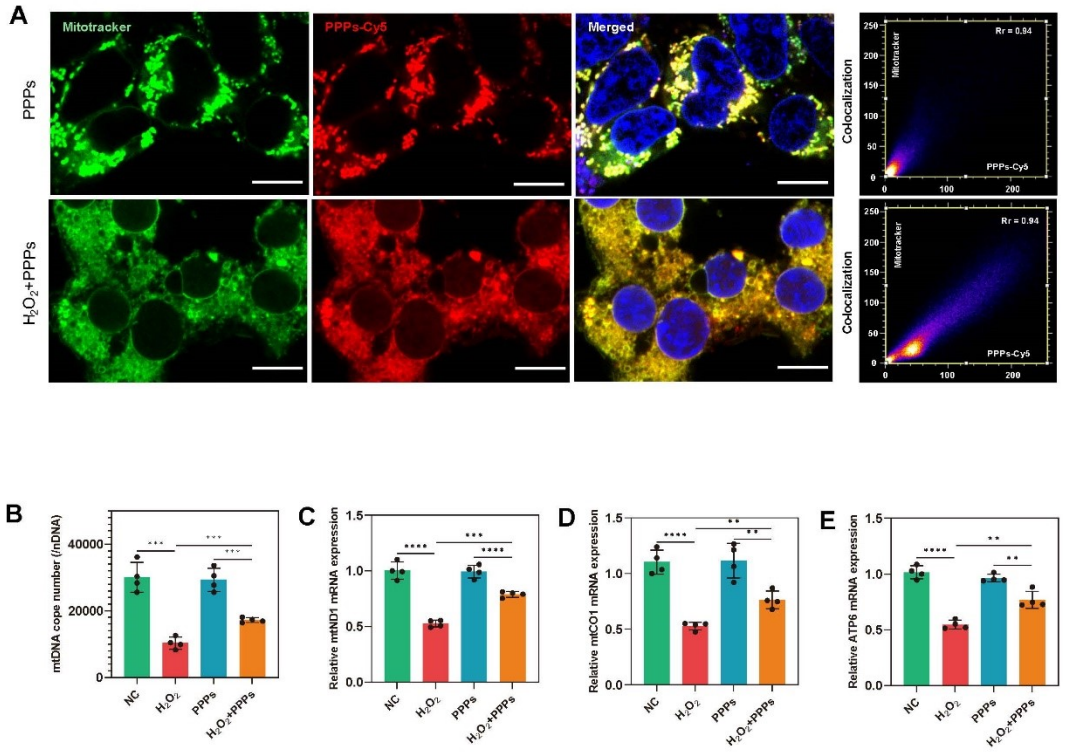

Figure S11. (A) Colocalization images of live HEK 293T cells at different treatments stained with Mitotracker (green) and PPPs-Cy5 (red). (B) The copy number of mtDNA. Mitochondrial mRNA of ND1 (C), CO1 (D) and ATP6 expression (E) were quantified and plotted relative to 18S control. Scale bar: 10 μm. $n = 4$ per group. $^{**}p < 0.01$, $^{***}p < 0.001$, and $^{****}p < 0.0001$.

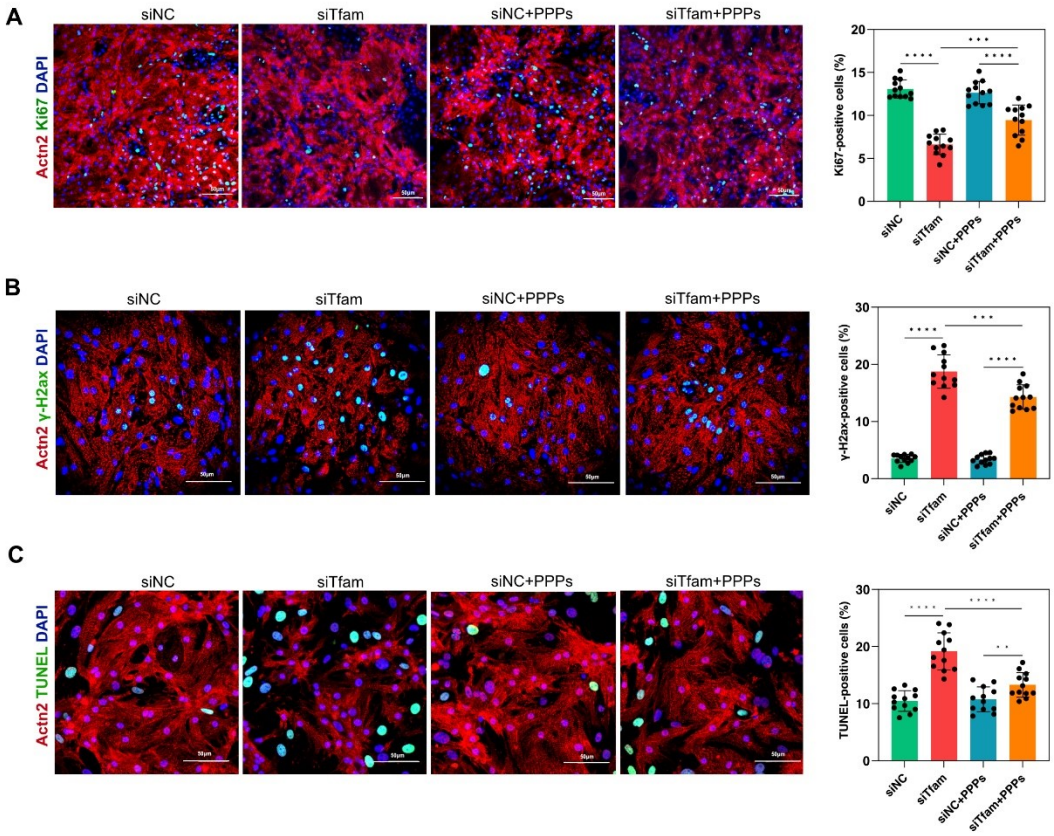

Figure S12. (A) Representative fluorescence microscopy images of NMVWs under various treatments stained with *Ki67*. (B) Representative fluorescence microscopy images of NMVWs under various treatments stained with *γ-H2ax*. (C) Representative fluorescence microscopy images of NMVWs at different treatments stained with TUNEL. Scale bar: 50 μm. $n = 12$ per group. *$p < 0.05$, **$p < 0.01$, ***$p < 0.001$, and ****$p < 0.0001$.

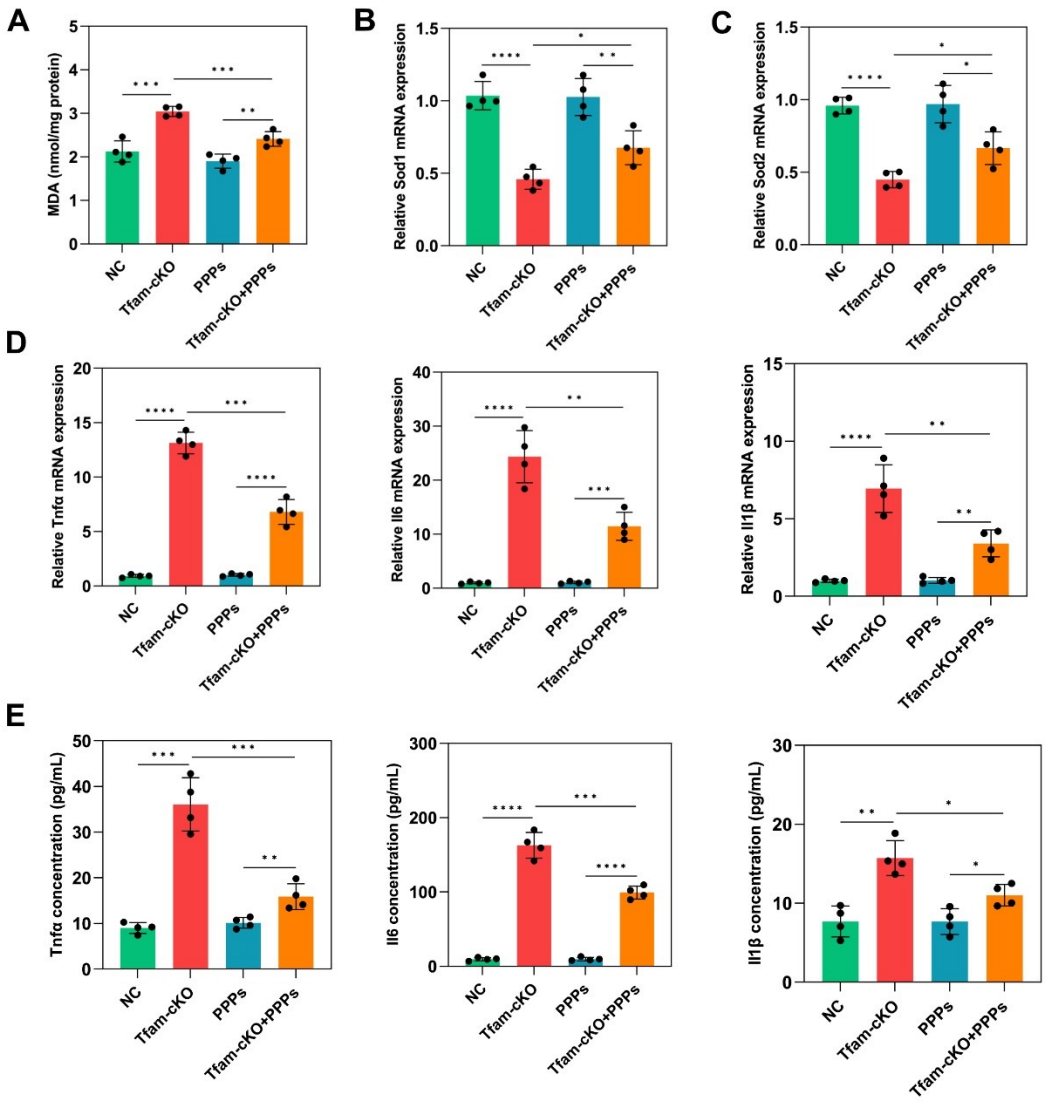

Figure S13. Levels of MDA (A), *Sod1* (B), and *Sod2* (C) in mouse hearts under various treatments (n = 4 per group). (D) The relative mRNA expression of inflammatory factors (*Tnfα, Il6 and Il1β*) of mouse hearts in various treatments (n = 4 per group). (E) The results of ELISA indicated that PPPs effectively decreased the secretion of mouse plasma inflammatory factors (n = 4 per group). *$p < 0.05$, **$p < 0.01$, ***$p < 0.001$, and ****$p < 0.0001$.

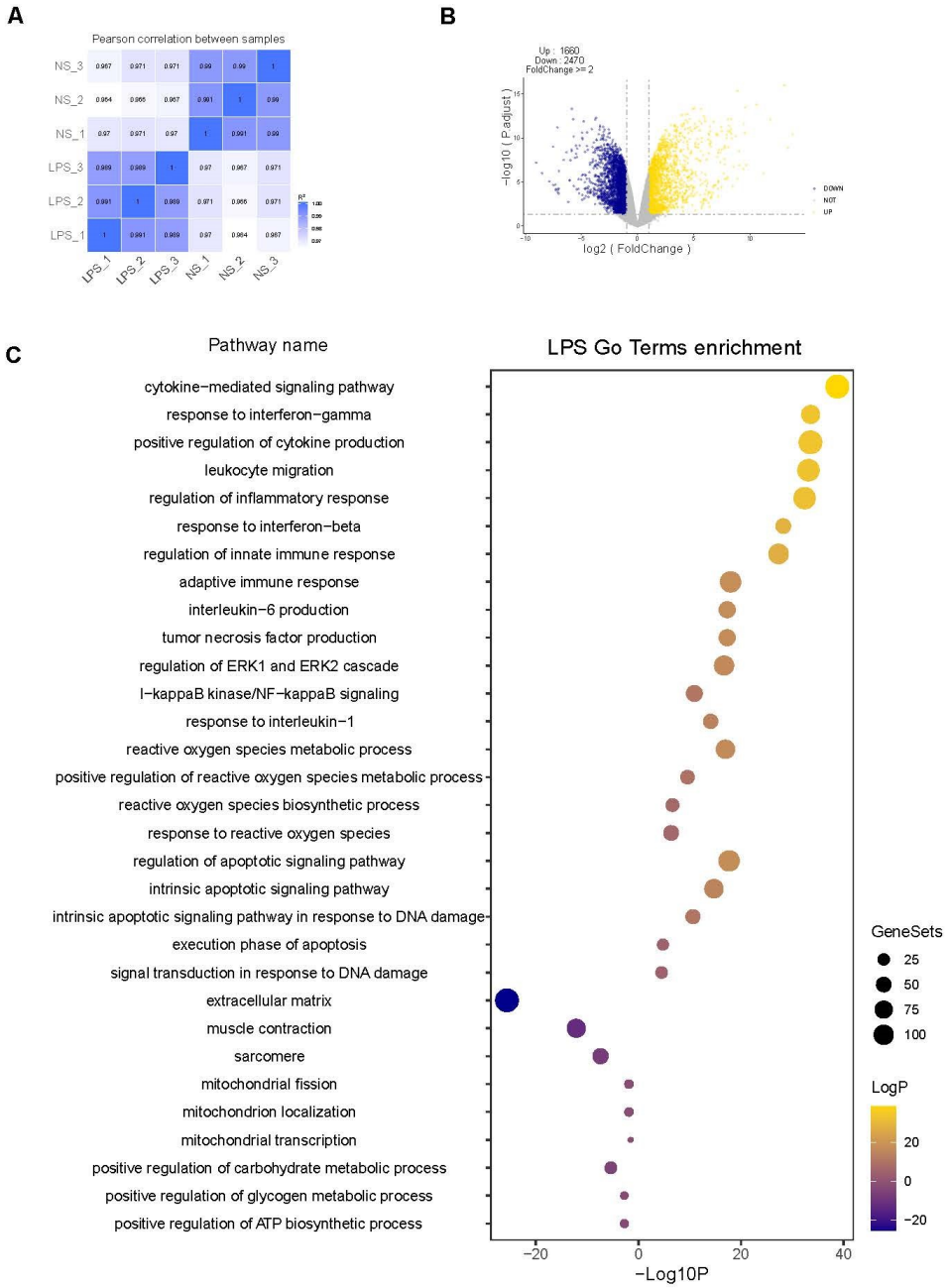

Figure S14. (A) Logarithm-transformed counts from an RNA-Seq dataset of saline- or LPS-treated myocardium, computed for sample correlation or variance using Pearson's correlation coefficient. (B) A volcano plot was illustrated with –log10(FDR) against log2FoldChange of all 4130 detected genes in the RNA-Seq dataset. Differential expression (DE) of genes were highlighted in blue and yellow to denote 2470 down-regulated and 1660 up-regulated genes, respectively. The significance of differential gene expression was assessed using an adjusted p-value (padj.) < 0.05 and counts > 50. (C) The GO terms were derived from analyzing all 4130 genes (n = 3 per group).

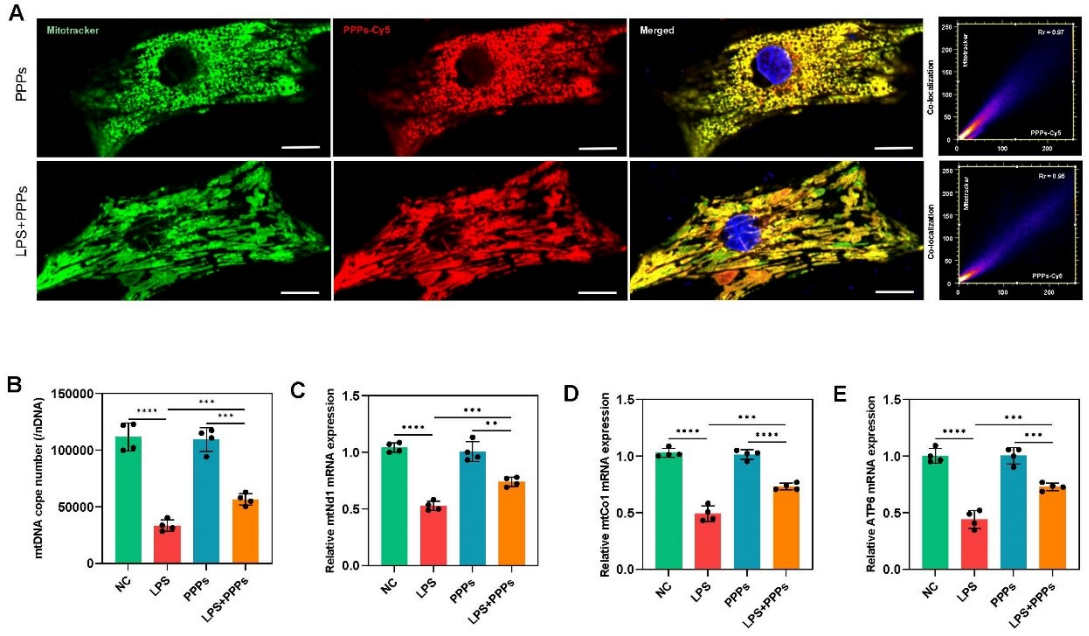

Figure S15. (A) Colocalization images of live CMs at different treatments stained with Mitotracker (green) and PPPs-Cy5 (red). (B) The copy number of mtDNA. Mitochondrial mRNA of Nd1 (C), Co1 (D) and ATP6 expression (E) were quantified and plotted relative to 18S control. Scale bar: 10 μm. $n = 4$ per group. $^{**}p < 0.01$, $^{***}p < 0.001$, and $^{****}p < 0.0001$.

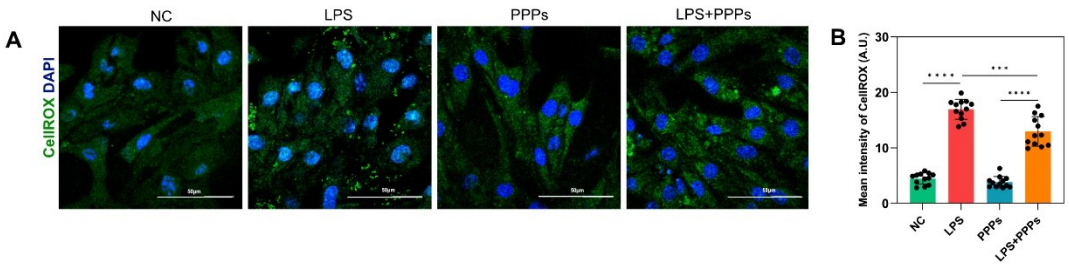

Figure S16. (A) Representative fluorescence microscopy images of CMs at different treatments stained with CellROX. Scale bar: 50 μm. (B) Quantitative analysis across replicates confirmed that PPPs markedly reduced CM ROS production (n = 12 per group). $^{*}p < 0.05$, $^{**}p < 0.01$, $^{***}p < 0.001$, and $^{****}p < 0.0001$.

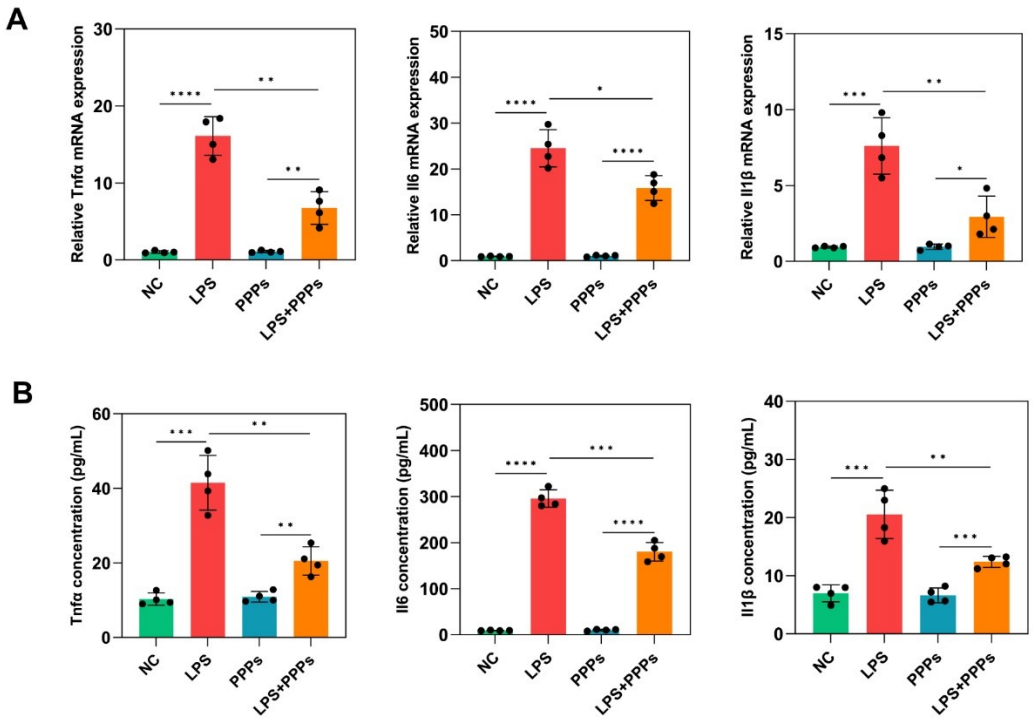

Figure S17. (A) The relative mRNA expression of inflammatory factors (*Tnfα, Il6 and Il1β*) of NMVWs in various treatments (n = 4 per group). (B) The results of ELISA indicated that PPPs effectively decreased the secretion of inflammatory factors in NMVWs (n = 4 per group). *$p < 0.05$, **$p < 0.01$, ***$p < 0.001$, and ****$p < 0.0001$.

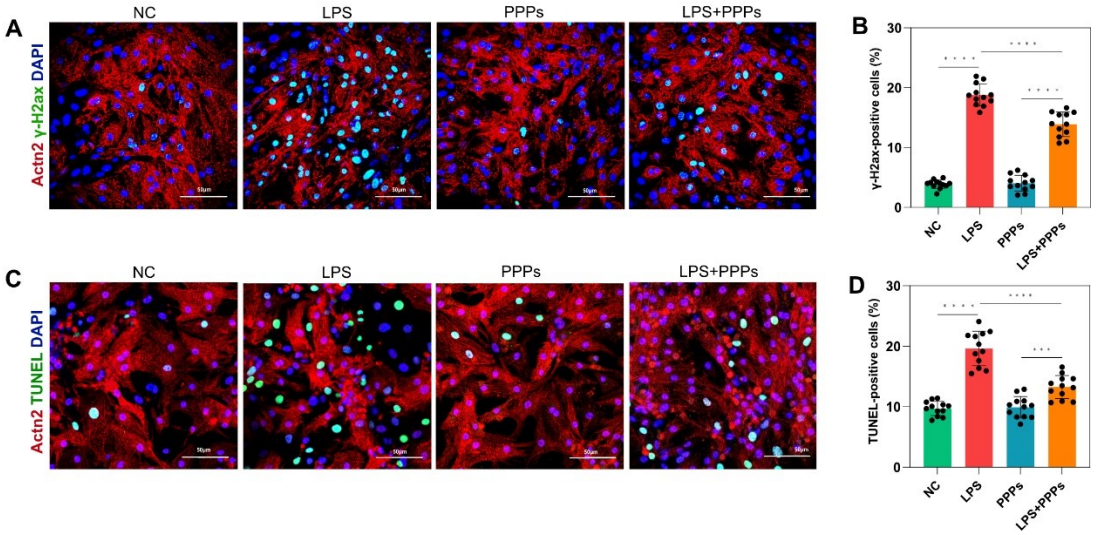

Figure S18. (A) Representative fluorescence microscopy images of NMVWs at different treatments stained with *γ-H2ax*. Scale bar: 50 μm. (B) The analysis of the proportion of *γ-H2ax* positive cells (n = 12 per group). (C) Representative fluorescence

microscopy images of NMVWs at different treatments stained with TUNEL. Scale bar: 50 μm. (D) The analysis of the proportion of TUNEL positive cells (n = 12 per group). *p < 0.05, **p < 0.01, ***p < 0.001, and ****p < 0.0001.

Table S1. Specific experimental conditions of PPP-i (i=1~4) NPs preparation.

Sample	Deionized water (mL)	Ethanol (mL)	HRP (μL)	H_2O_2 (mL)
PPP-1	18.55	3.75	140	2.70
PPP-2	16.25	3.75	260	5.00
PPP-3	14.45	3.75	350	6.80
PPP-4	12.05	3.75	480	9.20

Table S2. Several parameters of prepared PPP-i (i=1~4) NPs.

Sample	$Size_{SEM}$ (nm)	$Size_{DLS}$ (nm)	PDI	Zeta Potential (eV)	Yield (%)
PPP-1	104±7	134	0.101	-26.8	4.3
PPP-2	183±17	239	0.094	-24.1	9.5
PPP-3	268±14	325	0.138	-23.5	13.5
PPP-4	385±24	437	0.135	-23.3	18.4

Table S3. qRT-PCR primer sequences.

Gene	Primers	Sequences (5′–3′)
homo-mtDNA	Forward	ATACCCATGGCCAACCTCCTA
	Reverse	TAGGTTTGAGGGGGAATGCTG
homo-mtND1	Forward	GGCTATATACAACTACGCAAAGGC

	Reverse	GGTAGATGTGGCGGGTTTTAGG
homo-mtCO1	Forward	TCTCAGGCTACACCCTAGACCA
	Reverse	ATCGGGGTAGTCCGAGTAACGT
homo-ATP6	Forward	GAAGCGCCACCCTAGCAATA
	Reverse	GCTTGGATTAAGGCGACAGC
homo-SOD1	Forward	GGTGGGCCAAAGGATGAAGAG
	Reverse	CCACAAGCCAAACGACTTCC
homo-SOD2	Forward	GCTCCGGTTTTGGGGTATCTG
	Reverse	GCGTTGATGTGAGGTTCCAG
homo-TNFα	Forward	CCTCTCTCTAATCAGCCCTCTG
	Reverse	GAGGACCTGGGAGTAGATGAG
homo-IL6	Forward	ACTCACCTCTTCAGAACGAATTG
	Reverse	CCATCTTTGGAAGGTTCAGGTTG
homo-IL1β	Forward	ATGATGGCTTATTACAGTGGCAA
	Reverse	GTCGGAGATTCGTAGCTGGA
mus-mtDNA	Forward	CAACGCGGCAAACTAACCAA
	Reverse	CGATGTCTCCGATGCGGTTA
mus-mtNd1	Forward	CAACCATTTGCAGACGCCAT
	Reverse	TTGGGCTACGGCTCGTAAAG
mus-mtCo1	Forward	GCTAGCCGCAGGCATTACTA
	Reverse	CTCCGTGTAGGGTTGCAAGT
mus-ATP6	Forward	GCAGTCCGGCTTACAGCTAA
	Reverse	GGTAGCTGTTGGTGGGCTAA
mus-Tfam	Forward	ATTCCGAAGTGTTTTTCCAGCA
	Reverse	TCTGAAAGTTTTGCATCTGGGT
mus-Sod1	Forward	ATGGCGATGAAAGCGGTGT
	Reverse	CCTTGTGTATTGTCCCCATACTG
mus-Sod2	Forward	CAGACCTGCCTTACGACTATGG
	Reverse	CTCGGTGGCGTTGAGATTGTT
mus-Tnfα	Forward	CAGGCGGTGCCTATGTCTC
	Reverse	CGATCACCCCGAAGTTCAGTAG
mus-Il6	Forward	CTGCAAGAGACTTCCATCCAG
	Reverse	AGTGGTATAGACAGGTCTGTTGG
mus-Il1β	Forward	GAAATGCCACCTTTTGACAGTG
	Reverse	TGGATGCTCTCATCAGGACAG
homo/mus-18S	Forward	TTGACGGAAGGGCACCACCAG
	Reverse	GCACCACCACCCACGGAATCG